Structural Dynamics and Thermostabilization of Neurotensin Receptor 1

Sangbae Lee,[†] Supriyo Bhattacharya,[†] Christopher G. Tate,[§] Reinhard Grisshammer,[‡] and Nagarajan Vaidehi[†,*]

[†]Division of Immunology, Beckman Research Institute of the City of Hope, 1500 East Duarte Road, Duarte, California 91010, United States

[‡]Membrane Protein Structure Function Unit, National Institute of Neurological Disorders and Stroke, National Institute of Health, Department of Health and Human Services, Rockville, Maryland 20852, United States

[§]MRC Laboratory of Molecular Biology, Cambridge Biomedical Campus, Francis Crick Avenue, Cambridge CB2 0QH, U.K.

Supplementary Information

(A)

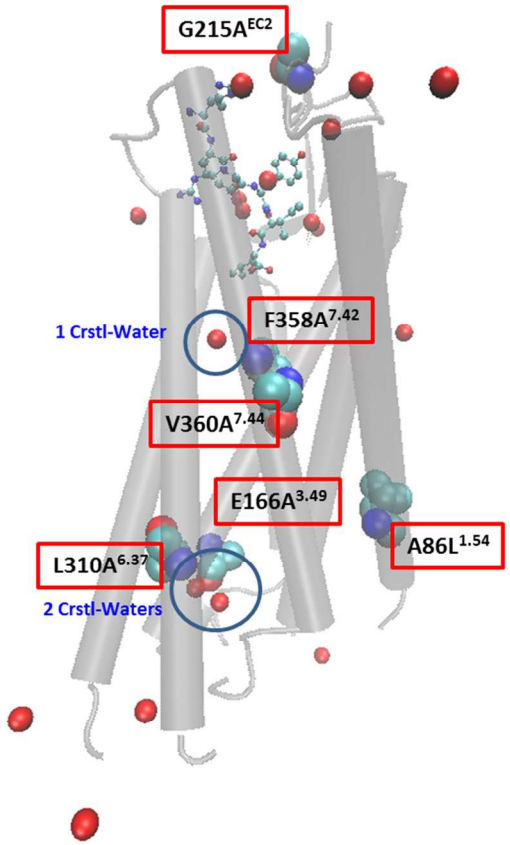

(B)

NTSR1 mutation	Stability relative to wild type NTS (=100%)
A86L$^{1.54}$	656
E166A$^{3.49}$	396
G215A^{ECL2}	348
L310A$^{6.37}$	520
F358A$^{7.42}$	760
V360A$^{7.44}$	399

Figure S1. The crystal structure information of the neurotensin receptor (NTSR1-4GRV). **(A)** The crystal structure of NTSR1-GW5 (called NTSR1-4GRV) including the six mutations (red box) and crystal waters within 4Å from each mutation (blue circles). **(B)** Experimental stability of single residue NTSR1 mutants measured in the presence of the full length [^{3}H]NTS. All experimental stability measurements are with respect to the stability of wild type NTSR1 and taken from Shibata et al. (2013).[(1)]

Table S1. The C_α distance between $R^{3.50}$ and $E(/L)^{6.30}$ in various crystal structures of GPCRs.

Receptor	Inactive State	Active State
β_2AR	11.2Å (2RH1)	17.2Å (3P0G), 18.0Å (3SN6)
A_{2A}R	7.3Å (3PWH), 9.7Å (3EML)	9.9Å (2YDO)
Rhodopsin	8.7Å (1GZM), 9.1Å (1U19)	14.5Å (2X72), 14.7Å (3PQR)
M_2	14.1Å (3UON)	15.5Å (4MQS), 15.8Å (4MQT)
δ-Opioid	9.3Å (4N6H)	
PAR1	9.0Å (3VW7)	
NTSR1	8.0Å (4BUO)	14.0Å (4GRV)

Table S2. Side chain distance of $P^{5.50}$ - $F^{6.44}$ in various crystal structures of GPCRs.

Receptor	Inactive State	Active State
β_2AR	7.8Å (2RH1)	5.6Å (3P0G), 5.1Å (3SN6)
A_{2A}R	7.6Å (3PWH), 7.9Å (3EML)	4.7Å (2YDO)
Rhodopsin	7.5Å (1GZM), 7.9Å (1U19)	4.2Å (2X72), 3.9Å (3PQR)
M_2	6.5Å (3UON)	5.1Å (4MQS), 5.3Å (4MQT)
δ-Opioid	12.3Å (4N6H)	
PAR1	3.8Å (3VW7)	
NTSR1	6.1Å (4BUO)	4.3Å (4GRV)

Table S3. Inter-residue distance between the alpha carbons of $R^{3.50}$ and $Y^{7.53}$ in various crystal structures of GPCRs.

Receptor	Inactive State	Active State
β_2AR	16.8Å (2RH1)	11.3Å (3P0G), 12.1Å (3SN6)
A_{2A}R	15.8Å (3PWH), 16.1Å (3EML)	11.6Å (2YDO)
Rhodopsin	15.8Å (1GZM), 15.5Å (1U19)	12.7Å (2X72), 12.8Å (3PQR)
M_2	17.6Å (3UON)	11.4Å (4MQS), 11.5Å (4MQT)
δ-Opioid	15.7Å (4N6H)	
PAR1	11.7Å (3VW7)	
NTSR1	15.9Å (4BUO)	11.9Å (4GRV)

Table S4. The center of mass (COM) distance of 5 residues in intracellular TM2 and TM6 in various crystal structures of GPCRs.

Receptor	Inactive State	Active State
β_2AR	18.2Å (2RH1)	26.6Å (3P0G), 29.7Å (3SN6)
A_{2A}R	19.4Å (3PWH), 19.0Å (3EML)	21.6Å (2YDO)
Rhodopsin	17.0Å (1GZM), 16.4Å (1U19)	24.9Å (2X72), 23.2Å (3PQR)
M_2	14.6Å (3UON)	25.8Å (4MQS), 26.0Å (4MQT)
δ-Opioid	17.7Å (4N6H)	
PAR1	17.9Å (3VW7)	
NTSR1	17.5Å (4BUO)	24.5Å (4GRV)

Table S5. Details of the different MD simulations on NTSR1 mutants and the wild type receptor.

	Ligand	Simulation Time	Lipid	Mutations
NTSR1-GW5	NTS_{8-13}	2,000 ns	POPC	$A86L^{1.54}$, $E166A^{3.49}$, $G215A^{ECL2}$, $L310A^{6.37}$, $F358A^{7.42}$, $V360A^{7.44}$
wt-NTSR1	NTS_{8-13}	2,000 ns	POPC	N/A
NTSR1-GW5-H8	NTS_{8-13}	2,000 ns	POPC	$A86L^{1.54}$, $E166A^{3.49}$, $G215A^{ECL2}$, $L310A^{6.37}$, $F358A^{7.42}$, $V360A^{7.44}$
wt-NTSR1-H8	NTS_{8-13}	2,000 ns	POPC	N/A

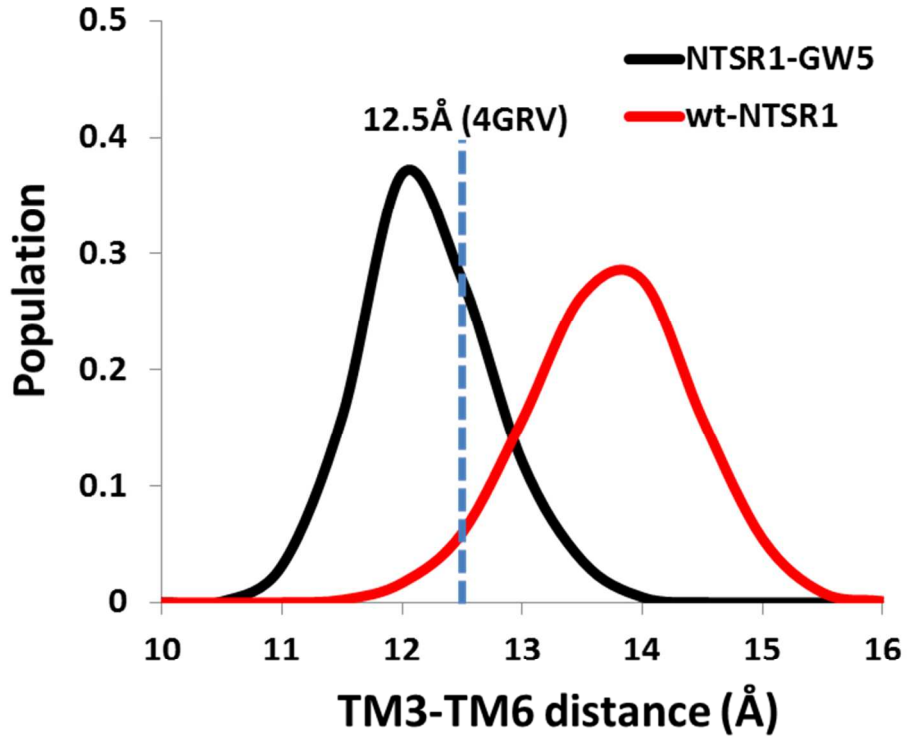

Figure S2. The TM3-TM6 distance between COM (center of mass) of the last 3 turns of the intracellular region of TM3 and TM6 for NTSR1-GW5 (black) and wt-NTSR1 (red) simulations.

(A)

	NTSR1-GW5 (kcal/mol)	Wt-NTSR1 (kcal/mol)	Δ(GW5-wt) (kcal/mol)
E(prot-ligand)	-465 (±8)	-457 (±11)	-8
E(prot-POPC)	-2,205 (±84)	-1,966 (±71)	-239
E(prot-water)	-71 (±11)	-41 (±9)	-30
E(prot)	-911 (±16)	-673 (±17)	-238
Total	-3,652 (±125)	-3,137 (±146)	-515

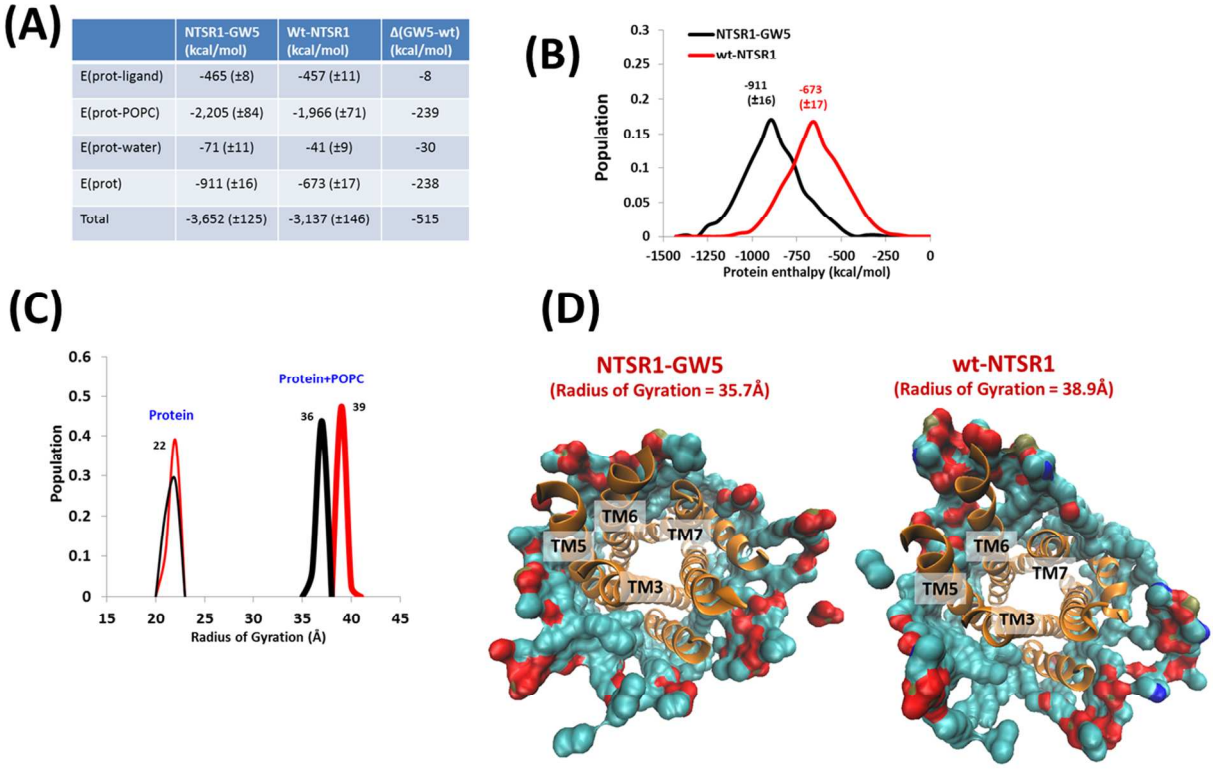

Figure S3. Calculated potential energy of the NTSR1-GW5 mutant and wt-NTSR1 receptor. **(A)** The protein energy and the protein-ligand, protein-POPC, and protein-water interaction energies are listed. The energy difference between NTSR1-GW5 and wt-NTSR1 is shown in last column. **(B)** Population distribution of protein potential energy for NTSR1-GW5 (black) and wt-NTSR1 (red). **(C)** Population distribution of the calculated radius of gyration which was calculated to analyze the lipid packing around the receptor. NTSR1-GW5 (black) and wt-NTSR1 (red). **(D)** A view of the lipid packing around the receptor of the representative structure from the most populated conformation cluster in the NTSR1-GW5 (left) and the wt-NTSR1 (right) (Intracellular view). The corresponding radius of gyration is also shown in this figure.

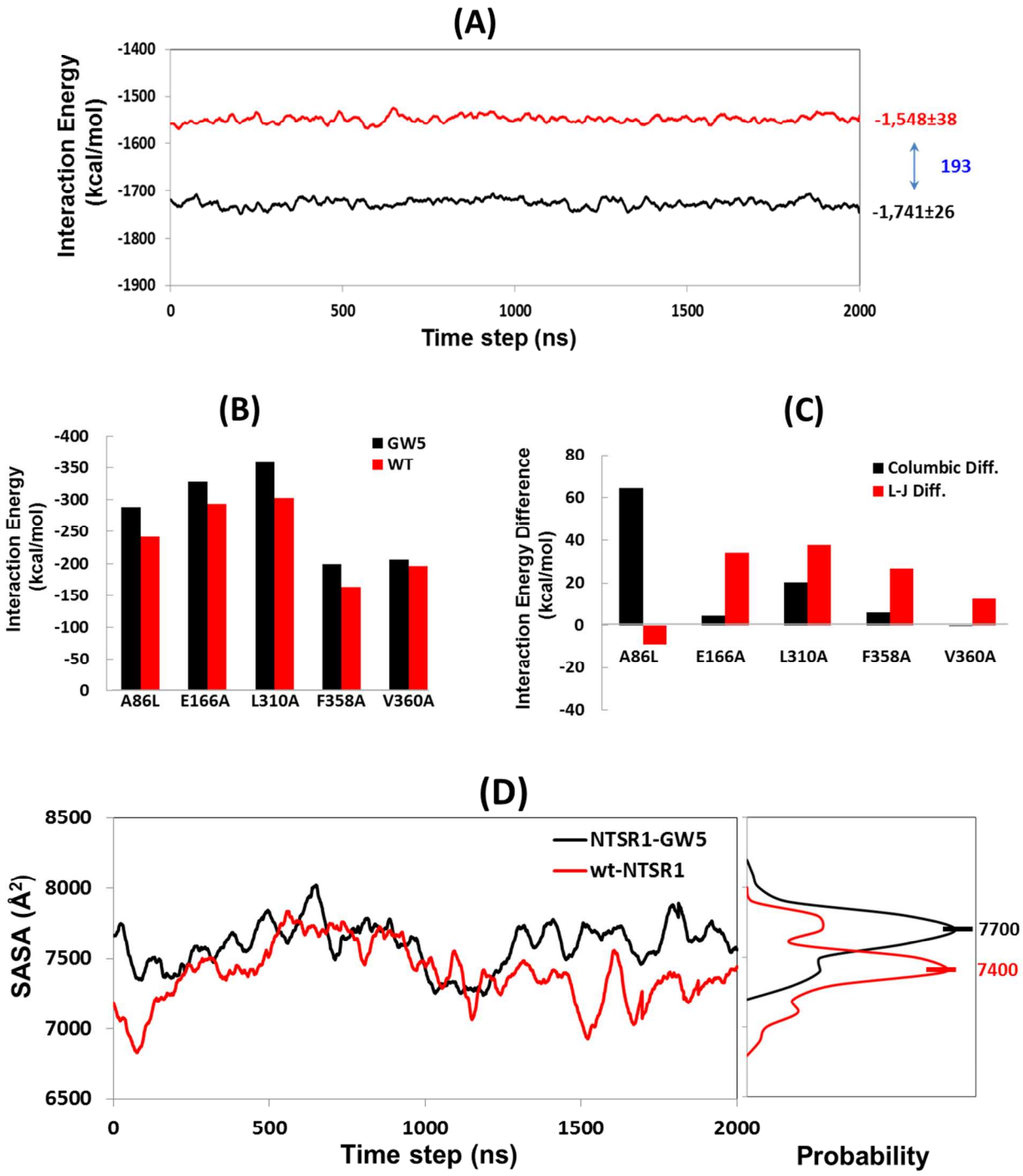

Figure S4. (A) The interaction energy between the lipid bilayer and the residues located within 7Å of the position of mutations in NTSR1-GW5 (black) and in the wild type (red). About 80% (193/239 kcals/mol) of the favorable interaction is retrieved by interaction of the residues within 7Å of the mutation positions. **(B)** Non-bonded interaction energies between lipid and the residues within 7Å of each the mutation positions (wt-NTSR1 shown in red and NTSR1-GW5 in black). **(C)** Difference in the Coulombic and van der Waals components of the lipid-protein interaction

energies between the NTSR1-GW5 and the wt-NTSR1, for the residues in the vicinity of each mutation positions. **(D)** The solvent accessible surface area of the protein regions that are exposed to the lipid bilayer (calculated as described in the Methods section) in the NTSR1-GW5 and wt-NTSR1.

Table S6. Residue pairs showing interhelical hydrogen bond interactions for NTSR1-GW5 and wt-NTSR1 simulations during 2 μs trajectories. The total number of hydrogen bond interactions is given within parenthesis in the column title.

	NTSR1-GW5 (#29)		wt-NTSR1 (#23)	
TM1-TM2	Y71-SC	E124-SC	Y71-SC	E124-SC
	N82-SC	A110-BB		
TM1-TM7	N82-SC	S362-BB		
	N82-SC	S362-SC		
TM2-TM3			T101-SC	E166-SC
	H105-SC	N159-SC	H105-SC	N159-SC
	H105-SC	S162-SC		
	S108-SC	N159-SC	S108-SC	N159-SC
			S112-SC	C152-BB
			S112-SC	T156-SC
	A120-BB	Y145-SC		
	E124-SC	Y145-SC		
	E124-SC	R149-SC	E124-SC	R149-SC
TM2-TM4	S108-SC	W194-SC	S108-SC	W194-SC
TM2-TM7	D113-SC	S362-SC	D113-SC	S362-SC
	D113-SC	N365-SC		
	M121-BB	Y359-SC		
	E124-SC	N355-SC	E124-SC	N355-SC
	E124-SC	Y359-SC	E124-SC	Y359-SC
TM3-TM4	R143-SC	L205-BB	R143-SC	L205-BB
	A155-BB	S197-SC	A155-BB	S197-SC
TM3-TM5	D150-SC	N241-SC	D150-SC	N241-SC
	Y154-SC	N241-SC	Y154-SC	N241-SC
	164-SC	N257-SC		
TM3-TM6	R149-SC	Y324-SC	R149-SC	Y324-SC
	D150-SC	R328-SC	D150-SC	R328-SC
TM3-TM7	R149-SC	N355-SC	R149-SC	N355-SC
	R149-SC	Y359-SC	R149-SC	Y359-SC
			R167-SC	S373-SC
TM5-TM6			N241-SC	R328-SC
	S245-SC	H325		
TM6-TM7	R327-SC	Y347	R327-SC	Y347-SC
	R327-SC	T354-SC	R327-SC	T354-SC
	R327-SC	N355-SC		

The residue pairs that are within 5Å of one of the six mutated residues and forming an interhelical hydrogen bond are listed. The notation, N355-SC represents that the side chain of N355. The abbreviations SC and BB are for side-chain and backbone atoms, respectively.

Table S7. Residue pairs showing interhelical van der Waals interaction in NTSR1-GW5 and wt-NTSR1 simulations during 2 μs trajectories.

	NTSR1-GW5	Total no. of interactions (#69)	wt-NTSR1	Total no. of interactions (#54)
TM1-TM2	T68	L125	T68	L125
	Y71	M121	Y71	M121
	F75	L117		
	F75	M121	F75	M121
	T79	L114		
			T85	A110
	A86L	A110		
	A86L	L114		
TM1-TM7	V67	M352	V67	M352
	Y71	Y359	Y71	Y359
	L74	A356		
			L74	Y359
	L74	V360A		
	L74	A363		
TM2-TM3			T101	T186
	V102	L163	V102	L163
			Y104	C172
	L106	L163		
	L109	T156	L109	T156
	L109	V160	L109	V160
	L109	L163		
			L115	C152
	I116	C152	I116	C152
	L119	L148	L119	L148
	A120	Y145		
	V123	Y145	V123	Y145
TM2-TM4	Y104	I190	Y104	I190
TM2-TM7	L106	Y369	L106	Y369
			L109	Y369
			I116	Y359
	L117	Y359		
	A120	Y359		
	M121	Y359		
TM3-TM4	Y146	M204		
	F147	A198		
	F147	A201	F147	A201
	F147	I202		
	F147	L205	F147	L205
	A151	A201		
	Y154	L200	Y154	L200
	A155	W194	A155	W194
	L158	I193	L158	I193
TM3-TM5			Y146	L256
	Y154	M244	Y154	M244
	A157	P249		
	V160	I253		
	V165	L256	V165	L256
	Y168	L256	Y168	L256
	Y168	V259	Y168	V259
	Y168	I260		
	I171	L264		
	C172	I260		
TM3-TM6	T153	W321	T153	W321
			T156	W321
	V160	V313		
TM3-TM7			Y146	Y351
			V160	Y369
TM4-TM5	T207	V237	T207	V237
TM5-TM6	V234	C332		
	I238	L329	I238	L329

	I238	C332	I238	C332
	F246	F317	F246	F317
	F246	W321	F246	W321
	F246	L322	F246	L322
	M250	F317		
	M250	V318	M250	V318
	I253	V314		
	I253	F317	I253	F317
			I260	A310
	A261	V307		
	L264	L303	L264	L303
	L264	V307		
			T265	L303
	T265	V307		
TM6-TM7			V309	L371
			V309	V372
			V313	L368
	V319	L357		
	C320	L357		
	C320	F358A		
			W321	F358
	P323	F350		
	P323	T354	P323	T354
	Y324	T354		
			Y324	F358
	M330	L343	M330	L343
			M330	F350
	F331	Y347	F331	Y347

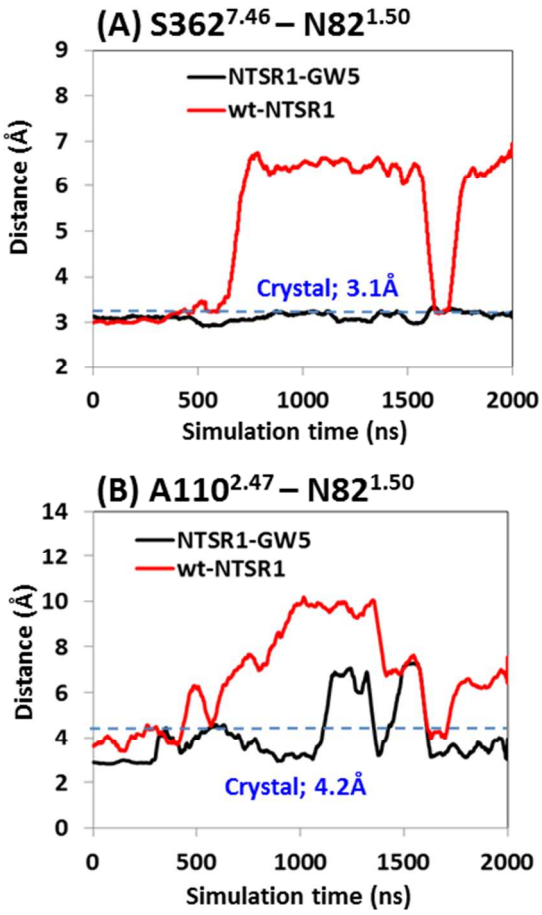

Figure S5. Interhelical hydrogen bond interactions close to A86L mutation in NTSR1-GW5 (black) and wt-NTSR1 (red). **(A)** S362$^{7.46}$(O) – N82$^{1.50}$(ND2), and **(B)** A110$^{2.47}$(O) – N82$^{1.50}$(ND2). Crystal structure distances for each interaction are shown as blue dotted-lines.

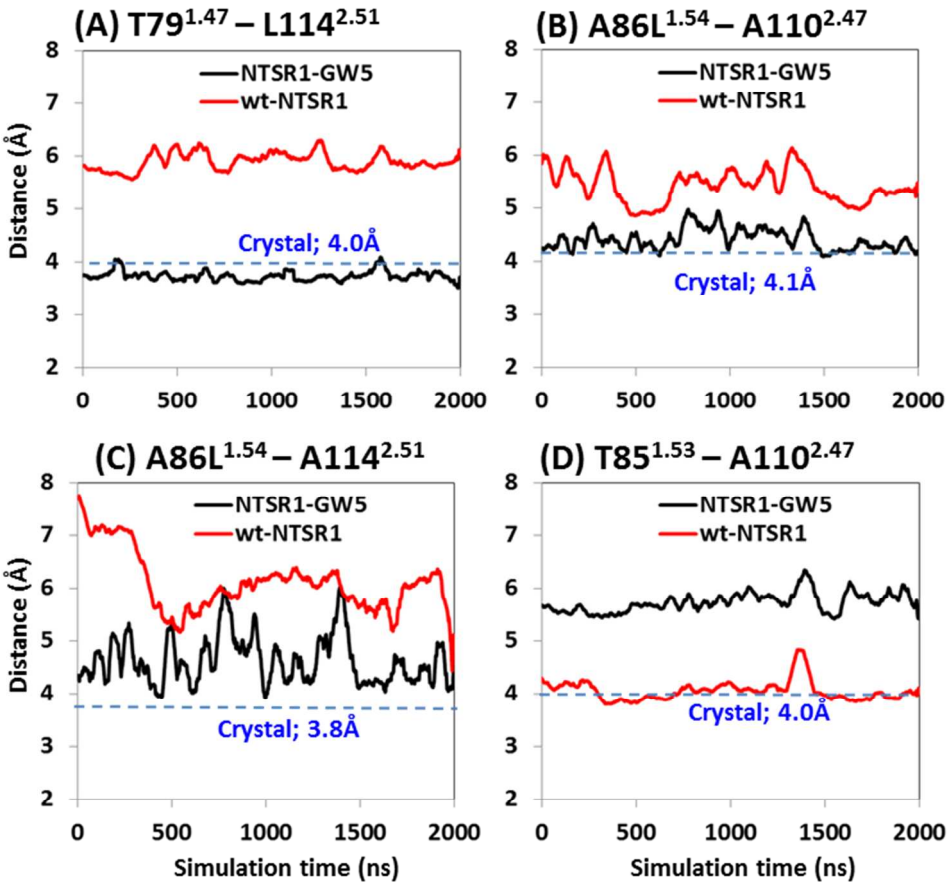

Figure S6. Time-dependent interhelical hydrophobic interactions near the A86L mutation in NTSR1-GW5 (black) and wt-NTSR1 (red). **(A)** T79$^{1.47}$ – L114$^{2.51}$, **(B)** A86$^{1.54}$ – A110$^{2.47}$, **(C)** A86L$^{1.54}$ – A114$^{2.51}$, and **(D)** T85$^{1.53}$ – A110$^{2.47}$. Crystal structure distances for each interaction are shown as blue dotted-lines.

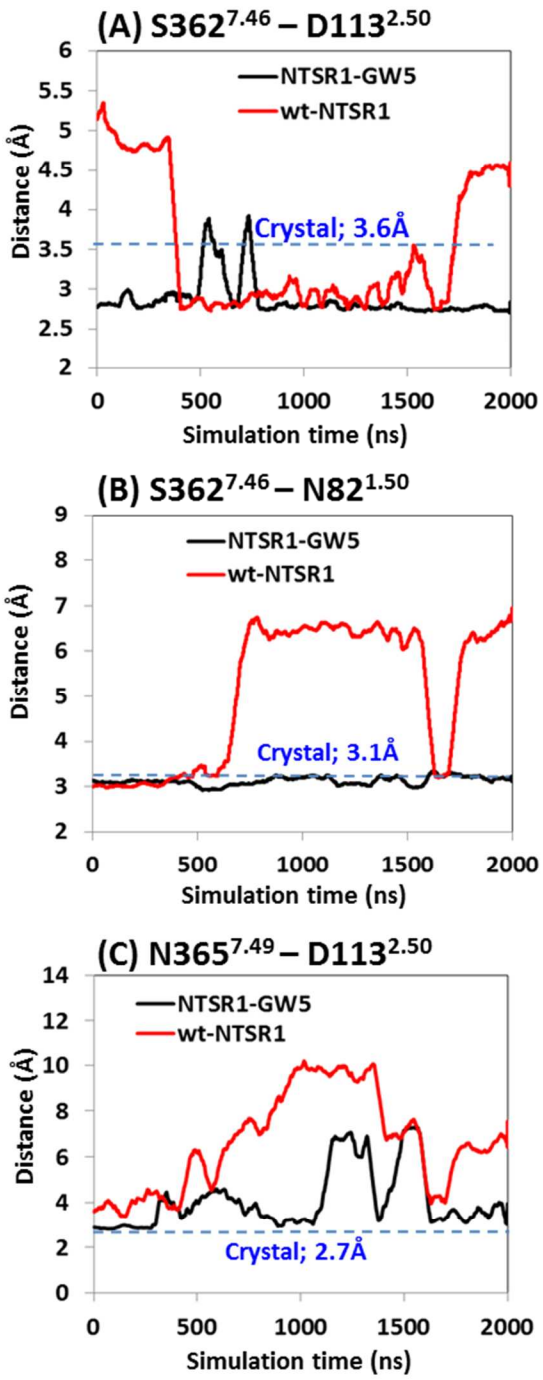

Figure S7. Interhelical hydrogen bond interactions near the V360A mutation in NTSR1-GW5 (black) and wt-NTSR1 (red). **(A)** S362$^{7.46}$(OG) – D113$^{2.50}$(OD*), **(B)** S362$^{7.46}$(O) – N82$^{1.50}$(ND2), and **(C)** N365$^{7.49}$(ND2) – D113$^{2.50}$(OD*). Crystal structure distances for each interaction are shown as dotted-lines.

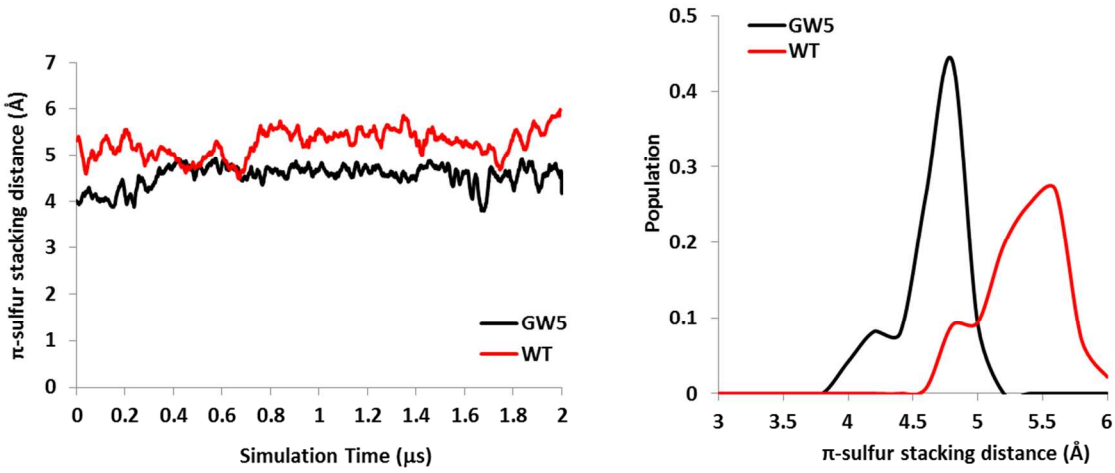

Figure S8. π-sulfur stacking pattern between M121$^{2.58}$ (Sulfur) and Y359$^{7.43}$ (center of mass of benzene ring) in NTSR1-GW5 (black) and wt-NTSR1 (red).

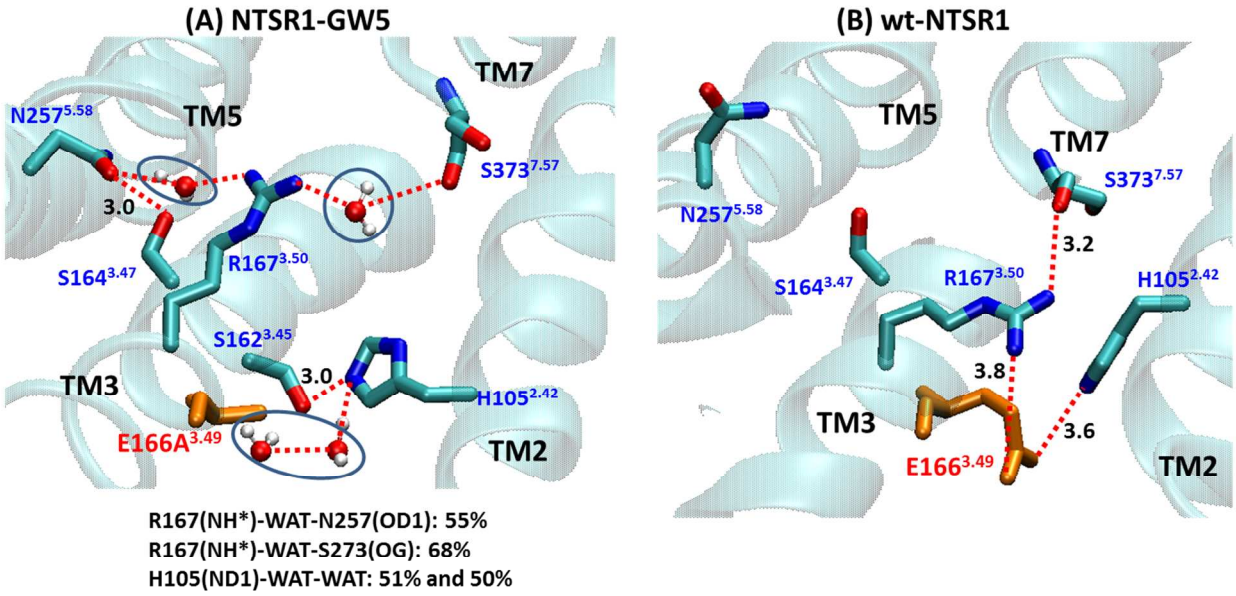

Figure S9. Effect of the mutation E166A$^{3.49}$ on the interhelical interactions in the neighborhood of the mutation. **(A)** Interhelical hydrogen bond interactions in NTSR1-GW5, and **(B)** corresponding snapshot in the wild type receptor. The percentage of the snapshots in the MD ensemble observed for each water is shown in the bottom of the figure.

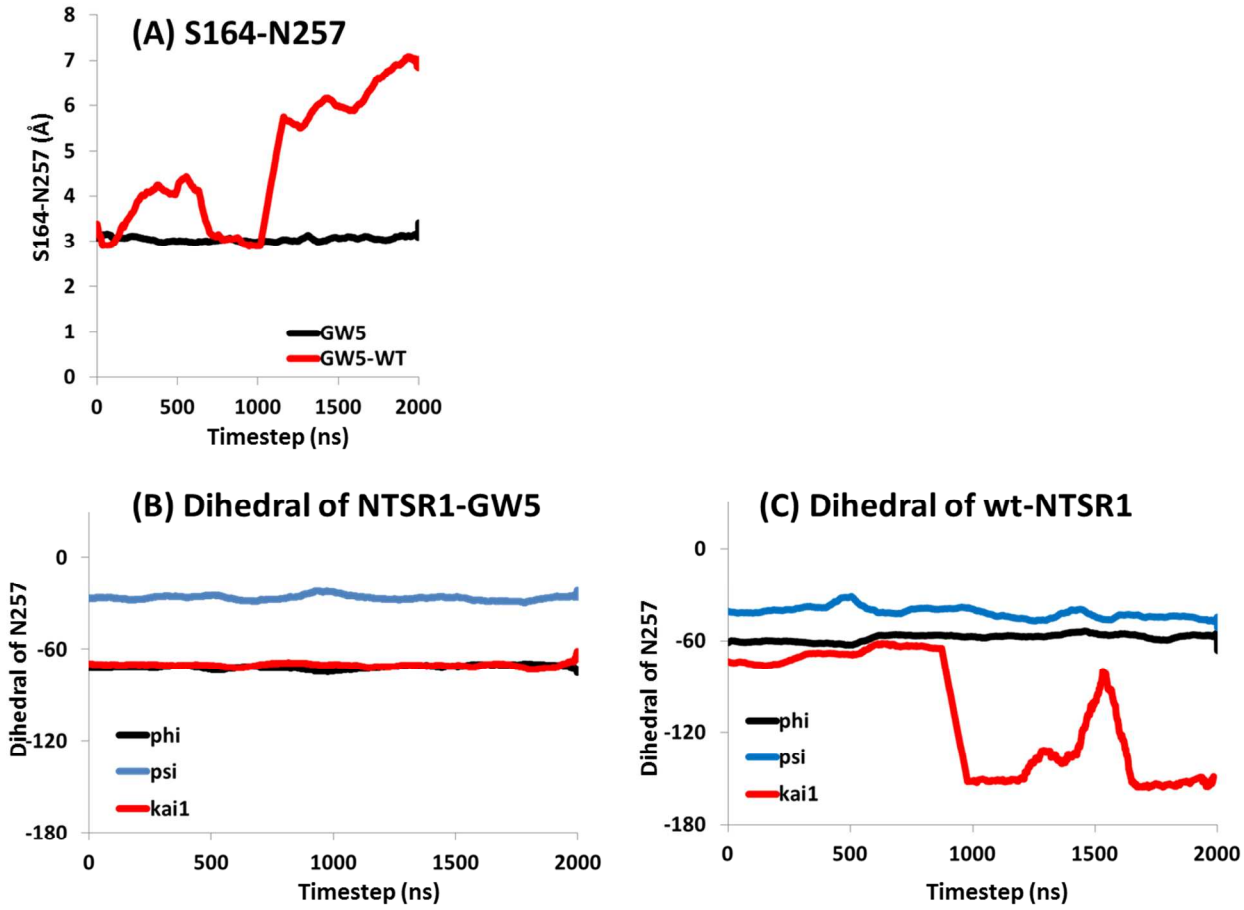

Figure S10. **(A)** The TM3-TM5 interhelical interaction as a function of time for S164$^{3.47}$ (TM3) and N257$^{5.58}$ (TM5). The distance between S164$^{3.47}$ (OG) and N257$^{5.58}$ (ND2) stays steady at the hydrogen bond interaction distance in NTSR1-GW5 (black) but breaks off in wt-NTSR1 (red). **(B & C)** The backbone and side chain dihedral angles of N257$^{5.58}$ in NTSR1-GW5 (B) and in wt-NTSR1 (C). The backbone dihedral *phi* and *psi* are shown as black and blue, and the side chain dihedral (*kai1*) is in red showing flexibility and rotation outwards.

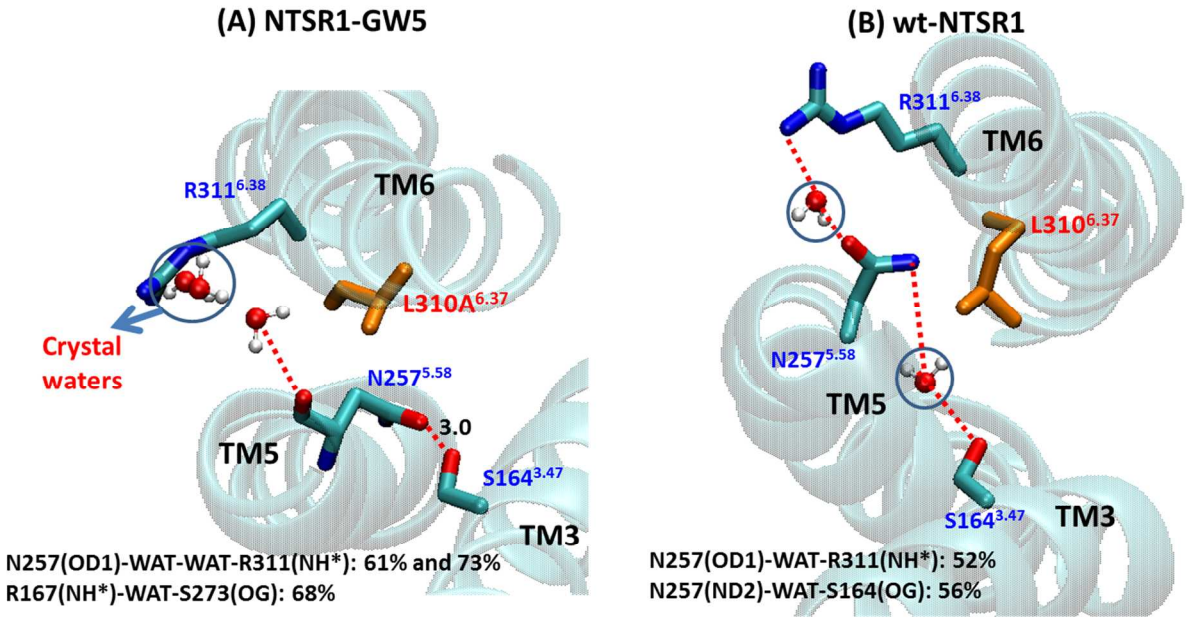

Figure S11. The effect of the mutation L310A$^{6.37}$ on the receptor thermostability. **(A)** The direct interhelical hydrogen bond interaction between N257$^{5.58}$ and S164$^{3.47}$ due to the neighboring mutation L310A$^{6.37}$ in NTSR1-GW5, and **(B)** the corresponding conformation in the wild type receptor. The percentage of the snapshots in the MD ensemble observed for each water is shown in the bottom of the figure.

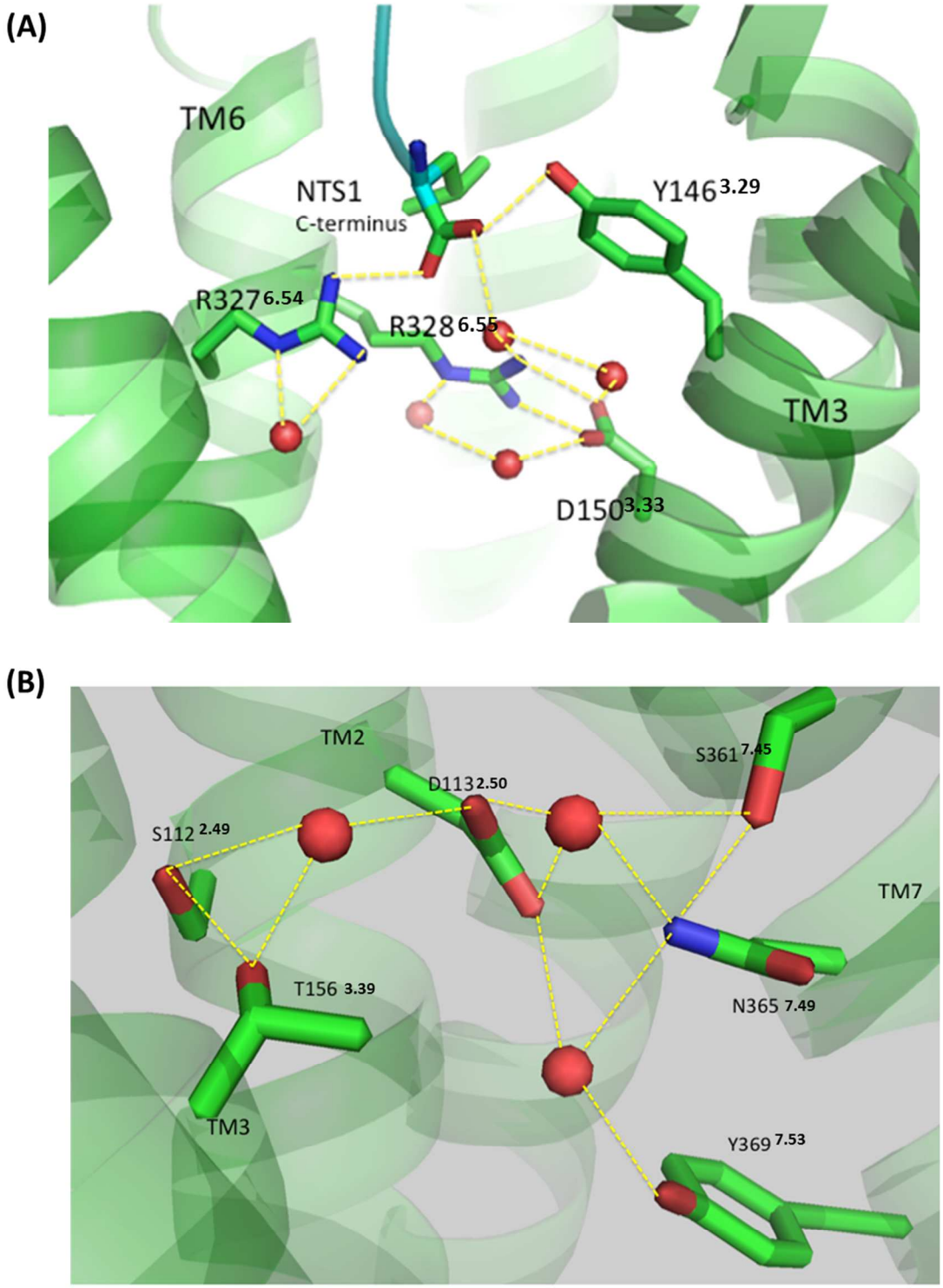

Figure S12. **(A)** Water clusters in NTSR1-GW5 forming hydrogen bond networks with the carboxy terminus of the NTS and the TM3 and TM6 in the extracellular region. **(B)** Water

mediated hydrogen bond networks between TM2, TM3 and TM7. All the distances shown in both the figures are within 3.5Å.

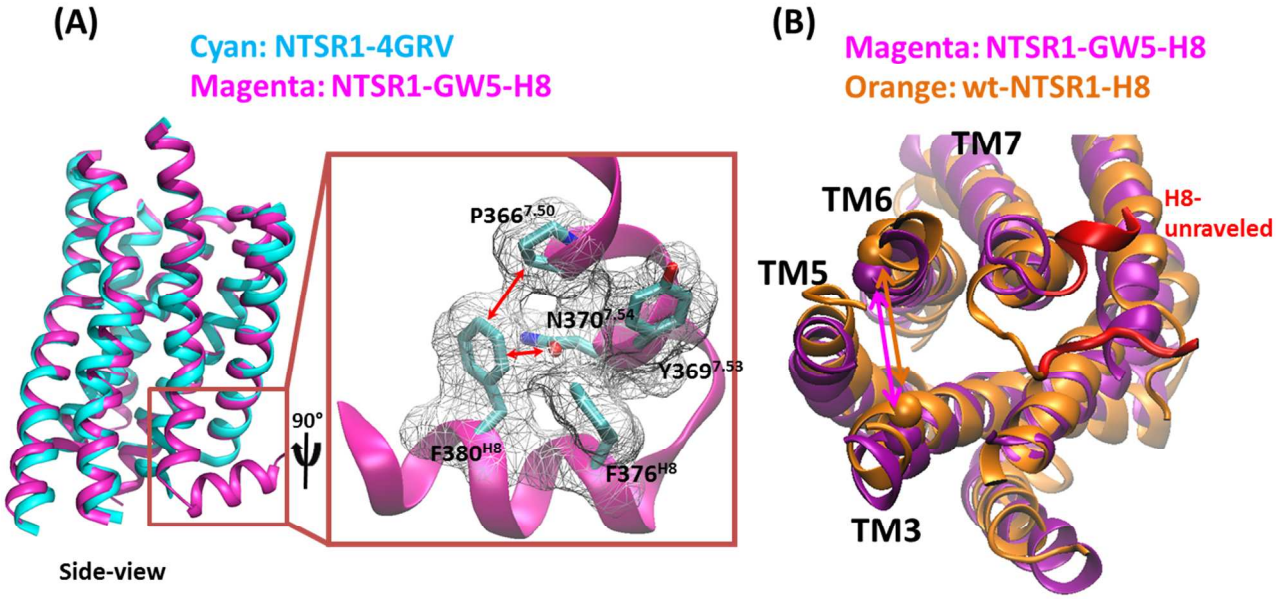

Figure S13. (A) Comparison of NTSR1-4GRV structure and the initial modeled NTSR1-GW5-H8. The NTSR1-4GRV crystal structure without helix 8 is shown in cyan and the equilibrated NTSR1-GW5-H8 with helix 8 built in is shown in magenta. Inset figure shows the steric hindrance between residues of TM7 and helix 8 in the NTSR1-GW5-H8 homology model. **(B)** Comparison of final snapshot of the homology models with addition of amphipathic helix 8. NTSR1 with helix 8 (NTSR1-GW5-H8) is shown in magenta, and wt-NTSR1-H8 is shown in orange. The unraveled helices 8 in NTSR1-GW5-H8 and in wt-NTSR1-H8 are shown in red color.

Table S8. Non-bonded interactions between residues of TM7 and helix 8 that would facilitate steric hindrance in the NTSR1-GW5-H8 homology model after equilibration.

	vdW interaction (kcal/mol)	Coulombic interaction (kcal/mol)	Min. contact distance (Å)
$P366^{7.50}$ – $F380^{H8}$	6.9	-1.5	4.0
$N370^{7.54}$ – $F380^{H8}$	6.6	-11.3	3.3

Table S9. The dynamics of residues in the helix 8 region during MD simulations of various class A GPCRs both in the inactive and active states. The residues highlighted in pink remain helical during MD simulations whereas residues with white background unraveled. The mustard colored structures are inactive states of various receptors and light-blue is in active or active-like states. The description of the systems is given in the table below.

Sequence of Helix 8 for various GPCR simulations																System used	
292I	293R	294E	295F	296R	297Q	298T	299F	300R	301K	302I	303I	304R	305S	306H	307V	wt-3PWH ($A_{2A}R$)	1
292I	293R	294E	295F	296R	297Q	298T	299F	300R	301K	302I	303I	304R	305S	306H	307V	3EML	2
444N	445A	446T	447F	448K	449K	450T	451F	452K	453H	454L	455L	456M				3UON (M2)	3
329S	330P	331D	332F	333R	334I	335A	336F	337Q	338E	339L	340L	341C	342L			2RH1 (β_2AR)	4
387N	388I	389E	390F	391R	392K	393A	394F	395L	396K	397I	398L	399S	400C			3PBL (D3)	5
472N	473E	474N	475F	476K	477K	478T	479F	480K	481R	482I	483L	484H	485I			3RZE (H1)	6
292I	293R	294E	295F	296R	297Q	298T	299F	300R	301K	302I	303I	304R	305S	306H	307V	wt-2YDO ($A_{2A}R$)	7
444N	445A	446T	447F	448K	449K	450T	451F	452K	453H	454L	455L	456M				4MQS (M2)	8
444N	445A	446T	447F	448K	449K	450T	451F	452K	453H	454L	455L	456M	457C			4MQT (M2)	9
329S	330P	331D	332F	333R	334I	335A	336F	337Q	338E	339L	340L	341C	342L	343R	344R	3P0G-wt (β_2AR)	10
374A	375N	376F	377R	378Q	379V	380F	381F	382S	383T	384L						NTSR1-GW5-H8	11
374A	375N	376F	377R	378Q	379V	380F	381F	382S	383T	384L						wt-NTSR1-H8	12

Secondary structure					
Magenta	Helix	White	Coiled		

	System used	Explanation
1	wt-3PWH ($A_{2A}R$)	Wild type simulation of Inactive $A_{2A}R$ bound to ZM241385 under POPC bilayer
2	3EML	A2A Adenosine receptor bound to ZM241385
3	3UON (M2)	M2 Muscarinic Acetylcholine receptor bound to Antagonist
4	2RH1 (β_2AR)	Human B2AR receptor bound to partial inverse agonist Carazolol
5	3PBL (D3)	Human dopamine D3 receptor in complex with D2/D3 selective antagonist Eticlopride
6	3RZE (H1)	Human Histamine H1 receptor in complex with first generation antagonist Doxepin
7	wt-2YDO($A_{2A}R$)	Wild type simulation of Active A2AR bound to Adenosine under POPC bilayer
8	4MQS (M2)	Active M2 Muscarinic Acetylcholine receptor bound to Agonist Iperoxo
9	4MQT (M2)	Active M2 Muscarinic Acetylcholine receptor bound to Agonist Iperoxo and allosteric modulator
10	3P0G-wt (β_2AR)	Wild type simulation of Nanobody-stabilized Active state of β_2AR
11	NTSR1-GW5-H8	Mutant Simulation of Neurotensin Receptor NTSR1 bound to agonist NTS peptide ligand
12	wt-NTSR1-H8	Wild type Simulation of NTSR1 bound to agonist peptide ligand

Blue	Active	Orange	Inactive

*The helix 8 region of NTSR1-TM86V (pdb code 4BUO) was found to less stable than that other GPCRs. [(2)]

The MD simulations on systems 1, 2 and 7 have been published in reference 3 of the Supporting Information.

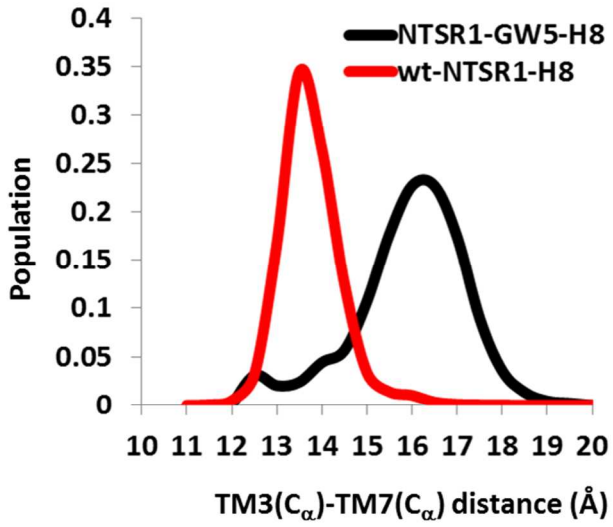

Figure S14. The population density variation with the inter-residue distance R3.50 – Y7.53 observed with the presence of helix 8 in the NTSR1-GW5-H8 (black) and the wt-NTSR1-H8 (red).

References

(1) Shibata, Y.; Gvozdenovic-Jeremic, J.; Love, J.; Kloss, B.; White, J. F.; Grisshammer, R.; Tate, C. G. *Biochim. Biophys. Acta.* **2013**, *1828*, 1293.

(2) Egloff, P.; Hillenbrand, M.; Klenk, C.; Batyuk, A.; Heine, P.; Balada, S.; Schlinkmann, K. M.; Scott, D. J.; Schutz, M.; Pluckthun, A. *Proc. Natl. Acad. Sci. U.S.A.* **2014**, *111*, E655.

(3) Lee, S.; Bhattacharya, S.; Grisshammer, R.; Tate, C.; Vaidehi, N. J. Phys. Chem. B. 2014, 118, 3355.